

# Fabrication and Characterization of Graphene/Graphene Oxide-Based Poly(vinyl alcohol) Nanocomposite Membranes

NGUYEN HUU HIEU,<sup>1,3</sup> NGUYEN HUYNH BACH SON LONG,<sup>2</sup>  
DANG THI MINH KIEU,<sup>1</sup> and LY TAN NHIEM<sup>1</sup>

1.—Faculty of Chemical Engineering, Ho Chi Minh City University of Technology, 268 Ly Thuong Kiet Street, District 10, Ho Chi Minh City, Vietnam. 2.—Faculty of Chemical and Environmental Engineering, Lac Hong University, 10 Huynh Van Nghe, Bien Hoa City, Dong Nai Province, Vietnam. 3.—e-mail: nhhieubk@hcmut.edu.vn

Graphene (GE)- or graphene oxide (GO)-based poly(vinyl alcohol) (PVA) nanocomposite membranes have been prepared by the solution blending method. Raman spectra and atomic force microscopy images confirmed that GE and GO were synthesized with average thickness of 0.901 nm and 0.997 nm, respectively. X-ray diffraction patterns indicated good exfoliation of GE or GO in the PVA matrix. Fourier-transform infrared spectra revealed the chemical fractions of the nanocomposite membranes. Differential scanning calorimetry results proved that the thermal stability of the nanocomposite membranes was enhanced compared with neat PVA membrane. Transmission electron microscopy images revealed good dispersion of GE or GO sheets in the PVA matrix with thickness in the range of 19 nm to 39 nm. As a result, good compatibility between GE or GO and PVA was obtained at 0.5 wt.% filler content.

**Key words:** Graphene, graphene oxide, poly(vinyl alcohol), nanocomposite, membrane

## INTRODUCTION

GE is a single layer of graphite, being found as layers of  $sp^2$ -hybridized carbon in the form of planar hexagonal rings corresponding to sigma-type bonds. In addition, the remaining  $p$ -orbitals form delocalized  $\pi$ -type bonds.<sup>1</sup>

In 2004, Geim and Novoselov discovered single-layer GE by using the scotch-tape method.<sup>1</sup> The structural model of single-layer GE is shown in Fig. 1.

GO is produced by oxidation of graphite, being a derivative of GE with oxygen-containing functional groups such as hydroxyl (–OH), epoxy (–COC–), carbonyl (–C=O), and carboxyl (–COOH).<sup>2</sup> The structural model of the surface and edges of GO is presented in Fig. 2.

GE has attracted a lot of attention in recent years because of its extraordinary physical and chemical

properties. Its properties include high electrical conductivity ( $200,000 \text{ cm}^2/\text{V-s}$ ), remarkable mechanical strength (Young's modulus  $\sim 125 \text{ GPa}$ ), excellent thermal conductivity ( $5000 \text{ W/m-K}$ ), and high specific surface area ( $2630 \text{ m}^2/\text{g}$ ).<sup>3,4</sup> In the case of GO, the oxygen functional groups have been found to be effective to enhance the chemical interactions between GO and other compounds.<sup>5</sup> In addition, GO sheets show increased interlayer spacing and solubility in water compared with GE.<sup>6</sup>

GE or GO can be used as a nanofiller in a polymer matrix to prepare nanocomposite membranes.<sup>7</sup> The good compatibility and dispersion of GE or GO sheets in polymers result in enhanced characteristics of such nanocomposite membranes.<sup>8–10</sup> In application of these nanocomposites for separation, the barrier property of the GE or GO sheets plays an important role in improving the membrane selectivity.<sup>11,12</sup> Simultaneously, the mechanical and thermal stability properties of the nanocomposite membranes are also enhanced, resulting in increased filtration efficiency.<sup>4,10–13</sup>

In this study, GE- or GO-based PVA membranes were fabricated by the solution blending method.<sup>10</sup> The effects of the GE or GO content on the morphology and structure of the GE/PVA and GO/PVA nanocomposite membranes were investigated by x-ray diffraction (XRD) analysis, transmission electron microscopy (TEM), Fourier-transform infrared (FTIR) spectroscopy, and differential scanning calorimetry (DSC). The obtained membranes are intended for dehydration of bioethanol solution by pervaporation technology.

## EXPERIMENTAL PROCEDURES

### Materials

PVA (molecular weight 80,000, degree >98%), sulfuric acid (98 wt.%), sodium nitrate (99 wt.%), hydrogen peroxide (30 wt.%), and hydrazine hydrate (35 wt.%) were purchased from Xilong Chemical, China. Graphite (particle size <50  $\mu\text{m}$ , density 20 g/100 mL to 30 g/100 mL) was purchased from Sigma Aldrich, Germany. Potassium permanganate (>99.5 wt.%) and ethanol (96 vol.%) were purchased from ViNa Chemsol, Vietnam. All chemicals were used without any further purification.

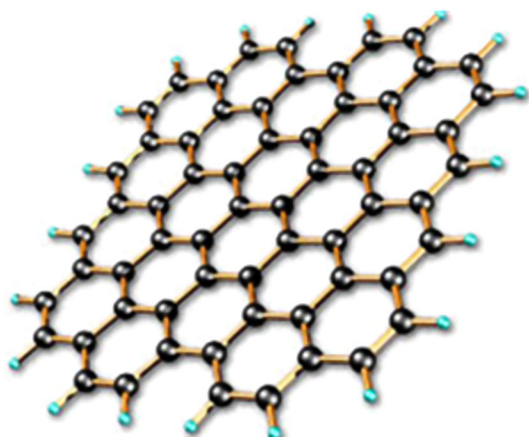


Fig. 1. Structural model of GE.<sup>1</sup>

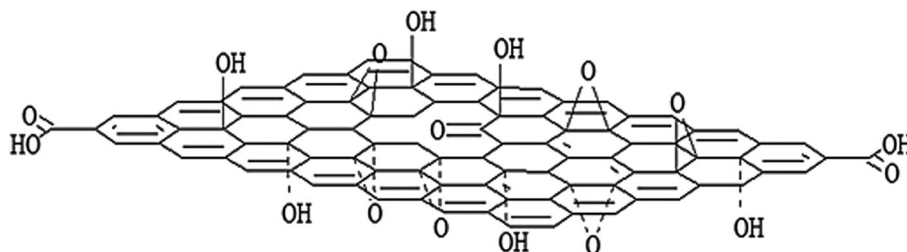


Fig. 2. Structural model of GO.<sup>2</sup>

### Fabrication of Nanocomposite Membranes

GE and GO were synthesized from graphite by a modified Hummers' method based on our previous study.<sup>13</sup> According to the solution blending method, 0.65 g PVA was dissolved in deionized water (100 mL) at 90°C. Then, 13 mL GE or GO aqueous suspension (0.25 mg/mL) corresponding to 0.5 wt.% (based on the weight of dry nanocomposite membrane) was dropped into the PVA solution and then stirred at 90°C for 1 h. The mixture was ultrasonicated at 45°C for 4 h to obtain a homogeneous suspension (GE/PVA or GO/PVA). Finally, the obtained suspension was cast onto glass Petri plates and dried at 90°C for 5 h. The nanocomposite membranes are denoted 0.5GE/PVA or 0.5GO/PVA, corresponding to the 0.5 wt.% of GE or GO.

The effect of the GE or GO content on the characteristics of the nanocomposites was investigated using different GE or GO loadings of 1.0 wt.%, 1.5 wt.%, and 2.0 wt.%. These membranes are denoted 1.0GE/PVA, 1.5GE/PVA, 2.0GE/PVA or 1.0GO/PVA, 1.5GO/PVA, 2.0GO/PVA for the corresponding GE or GO loadings.

### Characterization

Raman spectra were recorded using micro-Raman spectroscopy (LabRAM-HORIBA Jobin Yvon, excitation wavelength 632.8 nm). Atomic force microscopy (AFM) measurements were performed on an AFM Nanotec Electronica (Spain) on samples made by casting powder dispersions onto freshly cleaved mica substrates and drying under ambient condition. XRD patterns were recorded on an Advanced X8 Bruker machine at wavelength ( $\lambda$ ) of 0.154 nm in the Applied Material Science Institute. FTIR spectra were obtained in the wavenumber range from 4000  $\text{cm}^{-1}$  to 500  $\text{cm}^{-1}$  during 64 scans on an Alpha-E spectrometer (Bruker Optik GmbH, Ettlingen, German) in the Essential Laboratory of Chemical Engineering & Petroleum, Vietnam National University, Ho Chi Minh City University of Technology. DSC was conducted using a Mettler Toledo machine at linear heating rate of 40°C/min from 0°C to 240°C in the Laboratory of Membrane Technology. TEM images were taken using a JEM-1400 at accelerating voltage of 100 kV in the Essential Laboratory of Nanocomposite Materials.

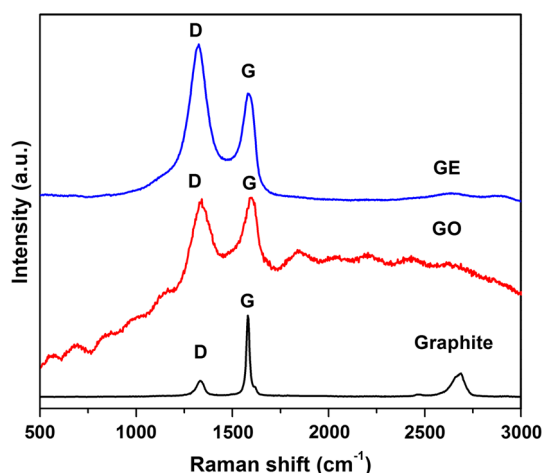


Fig. 3. Raman spectra of graphite, GO, and GE.

## RESULTS AND DISCUSSION

### Structure of GO and GE

Raman spectroscopy is widely used to characterize crystal structure, disorder, and defects in graphene-based materials. The Raman spectra of graphite, GO, and GE are shown in Fig. 3. The characteristic G-band and D-band peaks of graphite, GO, and GE were detected at around  $1580\text{ cm}^{-1}$  and  $1370\text{ cm}^{-1}$ , respectively. The G-band is related to vibration of  $sp^2$ -bonded carbon atoms in a two-dimensional hexagonal lattice. The D-band is associated with vibration of disordered  $sp^2$ -bonded carbon atoms.<sup>14,15</sup> These bands can be used to evaluate the extent of carbon-containing defects. The prominent D-band peak is from structural imperfections created by attachment of hydroxyl and epoxide groups on the carbon basal plane. The intensity of the D-band is related to the size of the in-plane  $sp^2$  domains.<sup>16</sup> Increase of the D-band peak intensity indicates formation of more  $sp^2$  domains.

Additionally, as seen in Fig. 3, the D/G intensity ratio for GE is larger than for GO (1.5 for GE and 1.0 for GO). This can be explained based on the fact that the relative intensity ratio of these peaks ( $I_D/I_G$ ) quantifies the degree of disorder and is inversely proportional to the average size of the  $sp^2$  clusters.<sup>16</sup> These results reveal that GO and GE were successfully synthesized, similar to previous works.<sup>14,15,17</sup>

AFM images and height profiles for GO and GE are shown in Fig. 4. Accordingly, the average thickness of the obtained GO and GE layers was found to be 0.901 nm and 0.997 nm, respectively. The AFM images confirmed that GO and GE were successfully synthesized, in agreement with previous studies ( $\sim 1\text{ nm}$ ).<sup>14,17</sup>

### Dispersion of GE or GO in PVA Matrix

The XRD patterns of GE, GE/PVA, GO, and GO/PVA membranes are shown in Fig. 5. The XRD

results indicate that the diffraction peaks for GE at  $2\theta = 21^\circ$  to  $26^\circ$  and for GO at  $2\theta = 11.27^\circ$  disappeared in the patterns of the nanocomposites. All typical diffraction peaks of GE/PVA and GO/PVA are located at  $2\theta = 19.46^\circ$  to  $20^\circ$ , corresponding to that of neat PVA at  $2\theta = 19.50^\circ$ .<sup>7,18</sup> These results demonstrate good incorporation and dispersion of GE or GO in the PVA matrix. Such incorporation improves the crystallinity of the PVA, as revealed by the increasing sharpness and width of the diffraction peaks.<sup>19,20</sup>

On the other hand, the improvement in crystallinity for the GO/PVA was greater than for the GE/PVA membranes. This can be explained by the fact that the GO sheets were almost completely dispersed in the PVA matrix through hydrogen bonds between the oxygen-containing groups in GO and hydroxyl groups in PVA.<sup>19,21</sup> Good crystallinity was achieved at 0.5 wt.% loading, corresponding to the highest and widest peaks in the pattern of GO/PVA. In the case of GE, the sheets of GE tend to aggregate and stack together. Such aggregation is attributed to the strong van der Waals interactions between the GE sheets. The formation of hydrogen bonds between the GE sheets and PVA matrix through some remaining oxygenated functionalities in GE is not strong enough to counterbalance the attractive van der Waals forces.<sup>21,22</sup> The appearance of aggregated GE sheets can restrict and order the PVA chain arrangement, causing the lower crystallinity of the GE/PVA membranes.<sup>8,19</sup> Furthermore, the peaks became weaker with increasing GE or GO content from 0.5 wt.% to 2 wt.%. This is due to the fact that, the higher the filler content, the more aggregation in the nanocomposites.<sup>22</sup>

Ultrathin sections of GE/PVA and GO/PVA membranes with 0.5% loading were observed via TEM. The images (Figs. 6 and 7) show good dispersion of aggregated GE or GO sheets in the PVA matrix with average thickness from 19 nm to 39 nm.

However, the GE sheets have higher density than those of GO due to the weak interaction between GE and PVA. These results are also consistent with the XRD patterns.

### Hydrogen-Bonding Interactions between GE or GO and PVA Matrix

The FTIR spectra of GE, GE/PVA, GO, and GO/PVA are shown in Fig. 8. The spectra show the characteristic peaks of various functionalities including alkyl ( $2942\text{ cm}^{-1}$ ), carbonyl ( $1712\text{ cm}^{-1}$  and  $1331\text{ cm}^{-1}$ ), and epoxy ( $1095\text{ cm}^{-1}$ ).<sup>14,19</sup> The peak located at  $1658\text{ cm}^{-1}$  is assigned to adsorbed water, indicating moisture intake in the membranes.<sup>12</sup> In all the spectra, the peaks located at  $3200\text{ cm}^{-1}$  to  $3500\text{ cm}^{-1}$  are attributed to stretching vibration of hydroxyl groups and hydrogen bonds.<sup>6,13</sup> Additionally, the spectra of GE/PVA show several small peaks located at  $3200\text{ cm}^{-1}$  to  $3500\text{ cm}^{-1}$  that can be ascribed to dissociation of hydrogen bonds

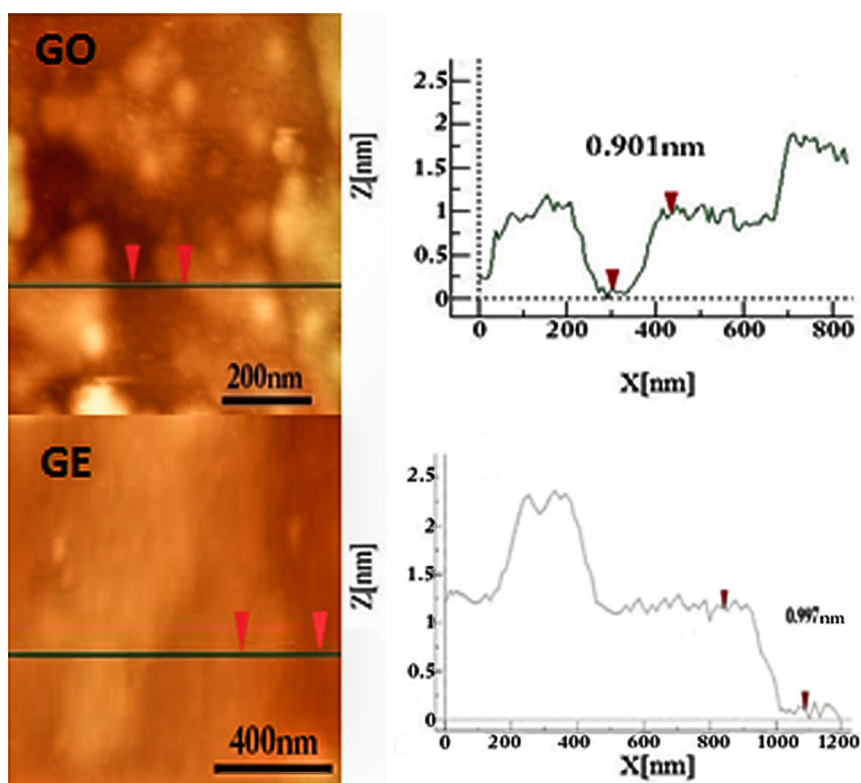


Fig. 4. AFM images and height profiles of GO and GE.

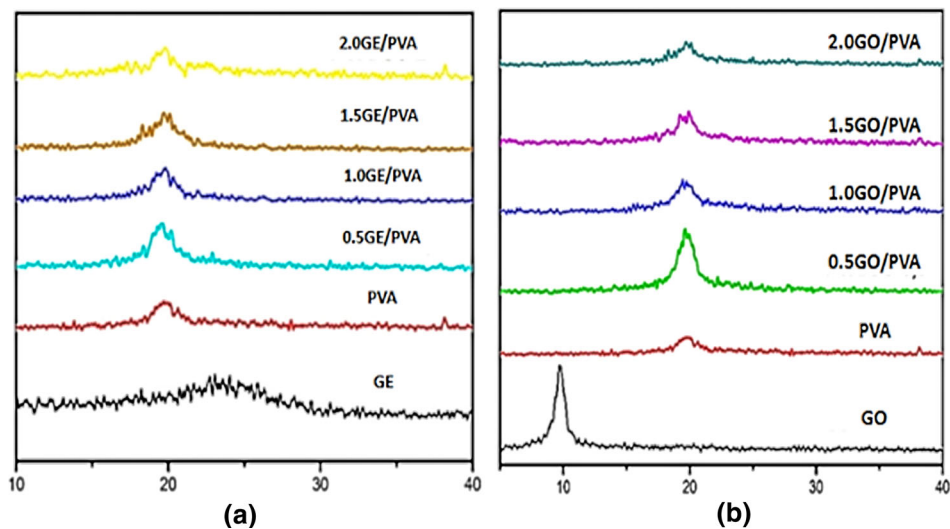


Fig. 5. XRD patterns of (a) GE and GE/PVA; (b) GO and GO/PVA.

among hydroxyl groups in PVA chains. This is due to intercalation of GE sheets, which cut off the hydrogen bonding between PVA chains, resulting in the unstable adsorption ability of GE/PVA.<sup>10,13</sup>

In contrast, in the case of GO, there is a decrease in the hydrogen bonding between the PVA chains due to the presence of the GO sheets. However, the total amount of hydrogen bonds in the GO/PVA is still larger than for neat PVA or GE/PVA.<sup>10,18</sup> This

can be attributed to the good dispersion and high compatibility between GO and the PVA matrix. Thus, the FTIR spectra of GO/PVA and neat PVA are similar, as shown in Fig. 8b.

### Thermal Properties of Membranes

The DSC results are presented in Table I. It can be seen that the glass-transition temperature  $T_g$  of



Fabrication and Characterization of Graphene/Graphene Oxide-Based Poly(vinyl alcohol) Nanocomposite Membranes

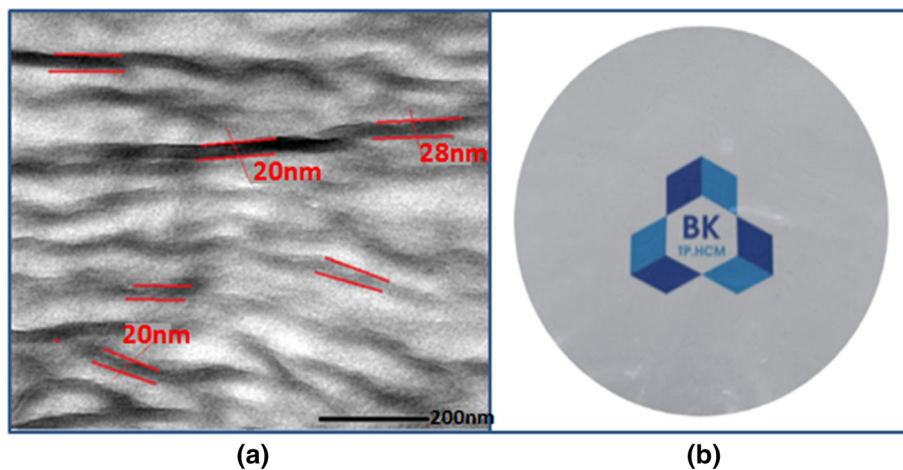


Fig. 6. (a) TEM image and (b) 0.5GE/PVA membrane product.

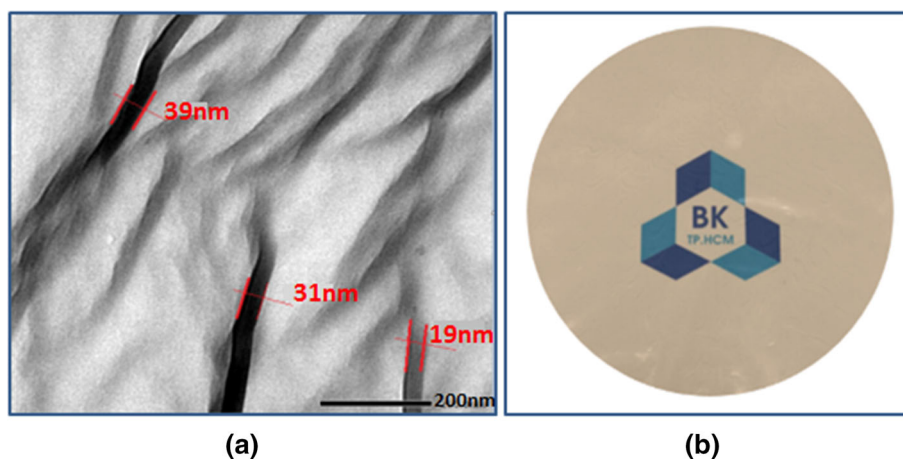


Fig. 7. (a) TEM image and (b) 0.5GO/PVA membrane product.

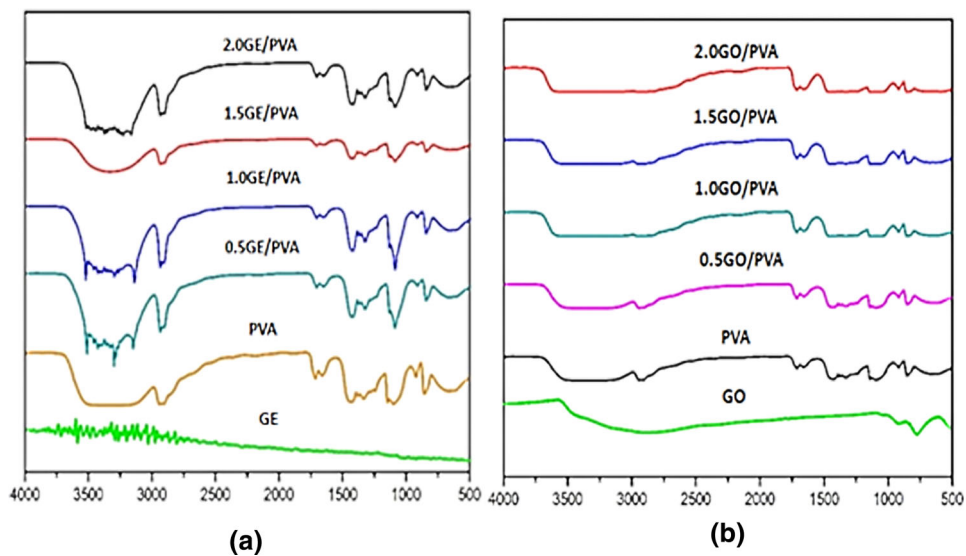


Fig. 8. FTIR spectra of (a) GE, GE/PVA and (b) GO, GO/PVA.

**Table I. Glass-transition temperature  $T_g$  of membranes**

Sample	$T_g$ (°C)	Sample	$T_g$ (°C)
PVA	57.34	0.5GE/PVA	80.27
0.5GO/PVA	60.42	1.0GE/PVA	82.31
1.0GO/PVA	65.53	1.5GE/PVA	83.68
1.5GO/PVA	67.15	2.0GE/PVA	86.70
2.0GO/PVA	70.34		

the nanocomposite membranes increased with addition of GE or GO. These results indicated that the thermal stability of the nanocomposites was enhanced compared with neat PVA. These results are in agreement with previous studies.<sup>8,13</sup> In addition, the  $T_g$  value for GO/PVA was lower than for the GE/PVA nanocomposites. This can be explained by the fact that the presence of abundant oxygen-containing functional groups in the GO sheets contributes to the good compatibility and dispersion of GO in the PVA matrix. However, the low thermal stability of these groups means that the polymer matrix is easily destroyed. Meanwhile, the high mechanical strength of GE leads to the enhancement of the thermal stability of GE/PVA, even though hydrogen bonds are not created in the nanocomposite.<sup>3,5</sup> Although the structure of the PVA crystals was changed due to the presence of GE or GO, the crystallinity was clearly improved. The DSC results show the important role of GE or GO in enhancing the thermal stability of the membranes.<sup>10,11</sup>

## CONCLUSIONS

GE/PVA and GO/PVA nanocomposite membranes were prepared by the solution blending method. The effects of GE or GO filler at 0.5 wt.%, 1 wt.%, 1.5 wt.%, and 2 wt.% loading on the characteristics of the membranes were investigated.

XRD analysis indicated that GO was more compatible with the PVA matrix compared with GE. TEM images showed that the filler sheets aggregated into multilayers. FTIR spectra demonstrated that the amount of hydrogen bonds in GO/PVA was much greater than in GE/PVA. A suitable content of GE or GO filler to prepare nanocomposite membranes was found to be 0.5 wt.%; and the dispersion of GO in the PVA matrix was better than that of GE.

DSC results revealed that the thermal stability of the nanocomposite membranes was enhanced in comparison with neat PVA membrane. In addition,

the  $T_g$  value of GE/PVA was higher than for GO/PVA.

The results indicate that nanoscale dispersion of GE or GO in the PVA matrix had a positive effect on the characteristics for both nanocomposite membranes.

## ACKNOWLEDGEMENT

The authors gratefully acknowledge the financial support from Ho Chi Minh City Department of Science and Technology through Contract No. 336/2013/HD-SKHCN.

## REFERENCES

1. K.S. Novoselov, V.I. Fal, L. Colombo, P.R. Gellert, M.G. Schwab, and K. Kim, *Nature* 490, 192 (2012).
2. D.R. Dreyer, S. Park, C.W. Bielawski, and R.S. Ruoff, *Chem. Soc. Rev.* 39, 228 (2010).
3. V. Singh, D. Joung, L. Zhai, S. Das, S.I. Khondaker, and S. Seal, *Prog. Mater. Sci.* 56, 1178 (2011).
4. C.M. Hassan and N.A. Peppas, *Adv. Polym. Sci.* 153, 37 (2000).
5. C. Bao, Y. Guo, L. Song, and H. Yuan, *J. Mater. Chem.* 21, 13942 (2011).
6. X. Yang, L. Li, S. Shang, and X.-M. Tao, *Polymer* 51, 3431 (2010).
7. H.-D. Huang, P.-G. Ren, J. Chen, W.-Q. Zhang, X. Ji, and Z.-M. Li, *J. Membr. Sci.* 409, 156 (2012).
8. K.J. Ramalingam, N.R. Dhineshbabu, S.R. Srither, B. Saravanakumar, R. Yuvakkumar, and V. Rajendran, *Synth. Met.* 191, 113 (2014).
9. M. Han, J. Yun, H.-I. Kim, and Y.-S. Lee, *J. Ind. Eng. Chem.* 18, 752 (2012).
10. A. Fahmy, M.A. Abu-Saied, E.A. Kamoun, H.F. Khalil, M. Elsayed Youssef, A.M. Attia, and F.A. Esmail, *J. Adv. Chem.* 11, 3426 (2015).
11. N.-W. Pu, C.-A. Wang, Y.-M. Liu, Y. Sung, D.-S. Wang, and M.-D. Ger, *J. Taiwan Inst. Chem. Eng.* 43, 140 (2012).
12. Y. Jin, M. Jia, M. Zhang, and Q. Wen, *Appl. Surf. Sci.* 264, 787 (2013).
13. A. Ammar, A.M. Al-Enizi, M.A. AlMaadeed, and A. Karim, *Arab. J. Chem.* (2015).
14. S. Stankovich, D.A. Dikin, R.D. Piner, K.A. Kohlhaas, A. Kleinhammes, Y. Jia, Y. Wu, S.T. Nguyen, and R.S. Ruoff, *Carbon* 45, 1558 (2007).
15. V. Loryuenyong, K. Totepvimarn, P. Eimburanaprat, W. Boonchompoo, and A. Buasri, *Adv. Mater. Sci. Eng.* 2013 (2013).
16. G. Sobon, J. Sotor, J. Jagiello, R. Kozinski, M. Zdrojek, M. Holdynski, P. Paletko, J. Boguslawski, L. Lipinska, and K.M. Abramski, *Opt. Express* 20, 19463 (2012).
17. J. Zhang, H. Yang, G. Shen, P. Cheng, J. Zhang, and S. Guo, *J. Chem. Commun.* 46, 1112 (2010).
18. T. Kuilla, S. Bhadra, D. Yao, N.H. Kim, S. Bose, and J.H. Lee, *Prog. Polym. Sci.* 35, 1350 (2010).
19. T. Zhou, F. Chen, C. Tang, H.-W. Bai, Q. Zhang, H. Deng, and Q. Fu, *Compos. Sci. Technol.* 71, 1266 (2010).
20. J. Chen, J. Huang, J. Li, X. Zhan, and C. Chen, *Desalination* 256, 148 (2010).
21. Q. Kang, J. Huybrechts, B. Van der Bruggen, J. Baeyens, T. Tan, and R. Dewil, *Sep. Purif. Technol.* 136, 144 (2014).
22. Y. Li, R. Umer, Y.A. Samad, L. Zheng, and K. Liao, *Carbon* 55, 321 (2013).